Data Analysis for GOPEX Image Frames

B. M. Levine
Optical Sciences and Applications Section

K. S. Shaik and T.-Y. Yan
Communications Systems Research Section

This article describes the data analysis based on the image frames received at the Solid State Imaging (SSI) camera of the Galileo Optical Experiment (GOPEX) demonstration conducted between December 9 and 16, 1992. Laser uplink was successfully established between the ground and the Galileo spacecraft during its second Earth-gravity-assist phase in December 1992. SSI camera frames were acquired which contained images of detected laser pulses transmitted from the Table Mountain Facility (TMF), Wrightwood, California, and the Starfire Optical Range (SOR), Albuquerque, New Mexico. Laser pulse data were processed using standard image-processing techniques at the Multimission Image Processing Laboratory (MIPL) for preliminary pulse identification and to produce public release images.

Subsequent image analysis corrected for background noise to measure received pulse intensities. Data were plotted to obtain histograms on a daily basis and were then compared with theoretical results derived from applicable weak-turbulence and strong-turbulence considerations. This article describes processing steps and compares the theories with the experimental results. Quantitative agreement was found in both turbulence regimes, and better agreement would have been found, given more received laser pulses. Future experiments should consider methods to reliably measure low-intensity pulses, and through experimental planning to geometrically locate pulse positions with greater certainty.

I. Introduction

This article describes the data analysis based on the image frames received at the Solid State Imaging (SSI) camera of the Galileo Optical Experiment (GOPEX) demonstration conducted between December 9 and 16, 1992. Simultaneous pulsed laser transmissions from the Table Mountain Facility (TMF), Wrightwood, California, and the Starfire Optical Range (SOR), Albuquerque, New Mexico, were recorded on the Solid-State Imaging (SSI) camera as a series of illuminated pixels in one image frame. Each pixel was quantized into 256 levels for transmission back to the JPL Multimission Image Processing Laboratory (MIPL) for processing. The image frames were transferred to the authors for analyses of the laser pulse strength.

A top-level summary of the GOPEX experiment, including statistics on the number of pulses received for each

day and for each frame, has been published separately,[1] and this article provides further results of statistical analyses. Section III describes image-processing techniques used at the MIPL and the custom procedures developed using the commercially available MATLAB software package to estimate laser pulse intensities, daily pulse-intensity histograms, and other relevant results. Software algorithms were written to identify each laser pulse and measure its strength above background. A statistical summary was compiled for each day's activities. These summaries were put in a form allowing comparison with an analytic model that predicts the probability distribution, and its moments for each night. Section IV provides a brief description for computing the lognormal variance for using either a weak turbulence theory or a strong turbulence theory. Section V provides a discussion comparing the experimental results with the statistical results using the parameters based on the statistical models discussed in Section IV.

II. GOPEX Summary

GOPEX was conducted on all but one evening between December 9 and 16 December, 1992. No operations were conducted on December 13, hence the data are reported according to days 1–4 and 6–8. On each night, pulsed lasers from TMF and SOR were directed toward the SSI camera of the Galileo spacecraft. During laser transmission, the scan platform of the SSI was activated (at approximately 6 mrad/sec) to spread the laser pulses in proportion to the telescope scan rate and the laser repetition rate. The TMF laser operated at 15 Hz for days 1 and 2, and at 30 Hz for the remainder of the experiment. SOR transmitted at 10 Hz during the days that laser pulses were detected. A simulated result for day 1 is shown in Fig. 1, as generated by MIPL. The two lines of pulses correspond to each transmission site. The distance between the lines is proportional to the distance between the two transmitting sites and the range to the spacecraft. The contrast in the figure has been digitally enhanced to exaggerate the relationship between the transmitting sites and the terminator, the location on the Earth in the shadow of the Sun's illumination. The image in Fig. 1 is displayed to correspond geographically with the more eastern SOR site, which is closer to the terminator. The distance between the transmitting sites and the terminator also changes in relation to the spacecraft range. The smearing of the terminator will influence the measurement of the laser pulse from its neighboring background illumination. This became a more significant factor in the later days of the experiment with a weaker laser signal and when the relatively large range placed both transmitters near the terminator and correspondingly closer to high background levels. Deviations in the laser pulse positions from a straight line were simulated from expected jitter of the scan platform. For the most part, the presence of laser pulses was identified with certainty by their separation from neighboring pulses. The simulated image served as the basis for all the image-analysis programs developed prior to the GOPEX demonstration.

[1] B. M. Levine, "GOPEX Data Products Summary," JPL Interoffice Memorandum (internal document), Optical Sciences and Applications Section, Jet Propulsion Laboratory, Pasadena, California.

III. Image Acquisition and Analysis

A. MIPL Image Acquisition and Processing

All GOPEX images were received at the MIPL according to a predetermined implementation plan.[2] During the first two days, the images were relayed to a real-time display from which identification of laser pulses could be made. Data display for the rest of the experiment was performed as soon as the images were played back from spacecraft storage. Images were modified by MIPL for pulse identification purposes during the first two days, and also for public release images. All data used to measure pulse energies were transmitted unmodified as 8-bit binary numbers for each pixel value. The disadvantage is that corrections for dark counts, responsivity uniformity, and individual pixel defects were not performed. The major reason for not correcting the GOPEX data was that the files used to make such corrections were out of date and would not be revised until significantly after GOPEX.[3]

Examples of raw and processed images are given in Fig. 2. The raw image contained numerous Reed–Solomon (RS) coding errors in the first two days of GOPEX. These errors appeared as horizontal bars across the frame and complicated a predetermined automated algorithm based on thresholding pixel values above the mean of each vertical column. The incidence of these errors practically disappeared after day 2, however, the intermittent incidence of errors forced the visual inspection of each frame to identify laser pulses throughout the remainder of the experiment.

B. Image Analysis

A set of programs to measure the intensity of all laser pulses was written in MATLAB [2], a commercial software

[2] L. Wanio, "SDT-MIPS GOPEX Implementation Plan–Version 2," JPL Interoffice Memorandum PA 6-384-92-LAW66.law (internal document), Jet Propulsion Laboratory, Pasadena, California, November 23, 1992.

[3] L. Wanio, private communication, Image Processing Applications and Development Section, Jet Propulsion Laboratory, Pasadena, California, November 1992.

package for numeric computation and data visualization. Program input consisted of a list of coordinate locations which specified the approximate peak of each pulse. One program would automatically find the centroid of the pulse and then would sum the data number (dn) values about a 5×5 window from the centroid. This size window was chosen because it encompassed the entire signal pulse found in the data simulations. Background would be subtracted by an average background 5×5 window which was computed from windows immediately to the left and right of the window containing the laser pulse data. It was originally desired to form the background window from data above and below the laser pulse window; however, the presence of coding error lines too frequently corrupted the result. In practice, signals above the background enclosed a 3×3 window because of the added noise in the actual data frames. A smaller window for adding all laser signals would have increased detection sensitivity. Additive measurement errors occur when a background measurement is subtracted from data containing both signal and background; thus, minimizing the window size would also minimize the accumulated measurement errors. After all calculations were made, the data were automatically separated into lists representing the two transmitter sites sorted by pixel location, and saved onto a file containing image analysis from all the day's image frames.

The result of such a calculation for the data illustrated in Fig. 2 is given in Table 1. The pulses attributed to SOR are uniformly spaced. The footnoted pulse numbers were added through calculations made independently of the computer program. In the case of TMF pulse 2, a modified value was substituted due to a line of dn's of 255 which corrupted the data. Originally the distance between pulse 5 and pulse 6 was 112.5 pixels, roughly equal to the distance between 3 laser pulses, as no pulses were visually observed on the thresholded image. Pulses 5.1 and 5.2 were added to the list from a hand calculation of the data about the expected location of the pulses.

For the exposure time of 800 msec, one would expect more pulses to be detected, up to 8 from SOR and up to 15 from TMF. It was suspected that the scan platform movement was not synchronized with the laser transmission times, which resulted in the loss of a number of pulses on each frame. Because of lack of correspondence between the exposure time and the expected number of laser pulses, it was not possible to correlate locations on the frame where no detection was recorded. This is important for two reasons. First, single detection events near a detection threshold cannot be reliably determined. This results in the under-reporting of pulses during the experiment. Second, there is a finite probability that the entire signal could be lost due to turbulence. Hence, the total number of zeroes is an important statistic in fitting histogram data to hypothesized probability distributions. The only certain way in which zero intensities could be determined is if they were to occur between two unambiguously identified laser pulses, as shown in the data in Table 1.

The other major program took a vector of intensity values for each day of GOPEX and plotted a histogram of dn values together with the expected lognormal probability distribution using parameter values determined from the analysis given in the next section, and also from the actual data. The results of all the histograms shown in this article were made by this program.

IV. Theoretical Development

The analytical model assumes that the optical beam possesses a Gaussian profile and the communication channel has lognormal scattering characteristics. The atmosphere-induced jitter is modelled as two independent zero-mean Gaussian random variables. By modelling the system parameters as a set of independent and identically distributed (iid) random variables, the combined impact of uncertainties due to system parameters and the turbulent atmosphere is approximated by a lognormal distributed signal intensity at the spacecraft [3].

The mean number of photoelectrons distributed over the pixels of the SSI camera has been computed for the laser uplink by Kiasaleh and Yan [3]. The corresponding lognormal variance, however, is not given, and must be computed separately from their analyses. The two theories given below provide the required lognormal variance. The first theory follows the work of Tatarski and is applicable only in the limit of weak turbulence, that is for a lognormal variance much less than unity. The seeing conditions at TMF during GOPEX were measured within this limit only on one of the observing nights. The second theory developed is applicable under conditions of strong atmospheric turbulence. It relies on statistically describing the effect of laser intensity fluctuations as a large number of strong independent disturbances on the received photoelectron count measured by the SSI. This limiting behavior was observed at TMF on all nights but one.

A. Weak Turbulence Theory

The lognormal variance taken from Tatarski [4] is given by

$$\sigma_N{}^2 = 2.24k^{-7/6}\sec(\theta)^{11/6}\int_0^z C_n^2(h)h^{5/6}dh \qquad (1)$$

where $k = 2\pi/\lambda$ is the wave number, θ is the zenith angle, $C_n^2(h)$ is the atmospheric structure constant, and z is the height of the atmosphere. Since no measurements of the atmospheric structure constant were made during the experiment, the above equation cannot be used to obtain good estimates of lognormal variance. However, rough estimates of seeing on the days when the GOPEX demonstration was conducted are available, and it is possible to rewrite Eq. (1) to make use of the seeing estimates. Assuming a zenith height, z_0, for the atmosphere, with $C_n^2(h)$ a constant, Eq. (1) simplifies to

$$\sigma_N{}^2 = 10.3\lambda^{-7/6} z^{11/6} C_n^2 \tag{2}$$

where $z = z_0 \sec(\theta)$. An expression for r_0, the atmospheric coherence parameter, is given below [5]:

$$r_0 = 0.185\ \lambda^2/(zC_n^2)^{\ 3/5} \tag{3}$$

Note that the seeing, α, can be simply related to the zenith atmospheric coherence length by the relation $\alpha = 4\lambda/(\pi r_o)$.[4] Eliminating C_n^2 from Eqs. (2) and (3), one gets

$$\sigma_N{}^2 = 0.4(z_0/\lambda)^{5/6} [\sec(\theta)\alpha^2]^{5/6} \tag{4}$$

Using this expression and assuming $z_0 = 7$ km with $\lambda = 0.532\ \mu$m, Eq. (4) can be further reduced to

$$\sigma_N^2 = 1.0 \times 10^8\ \sec(\theta)\alpha^{2\ \ 5/6} \tag{5}$$

Equation (5) calculates lognormal variance in terms of the seeing (in radians) and the zenith angle. This equation can now be used to compute log-variance from the estimated seeing for the GOPEX demonstration days. The lognormal mean, m_n, of the distribution is given by the expression

$$m_n = \ln < N_{tot} > \ - 1/2\sigma_N^2 \tag{6}$$

where $< N_{tot} >$ is the expected number of photoelectrons at the detector which can be calculated using the equations developed by Kiasaleh and Yan [3].

[4] K. S. Shaik, JPL Interoffice Memorandum 331.6-91-191 (internal document), Communications Systems Research Section, Jet Propulsion Laboratory, Pasadena, California, September 3, 1991.

B. Strong Turbulence Theory—Photoelectric Count Probability Distribution

Consider the charge-coupled device (CCD) on the SSI as a detector that converts incident photons into counts of photoelectrons. The amplifiers and digitizing circuitry that follow convert the photoelectron count into a dn value, depending on its system parameters. For the SSI, the photoelectron count can be associated to the dn by a gain state, g, which can be set over 4 different values. Specifically, the dn is related to the photoelectron count, $< N_{tot} >$, by the multiplicative relation

$$dn = gN_{tot} \tag{7}$$

Thus, photoelectron counts are discussed interchangeably with dn values in the following discussion. Statistical errors from the quantization noise introduced by Eq. (7) have been ignored.

A photoelectric detector, such as a CCD, generates counting statistics which obey the Poisson probability law, and furthermore the parameter of the Poisson distribution is proportional to the light intensity. Thus, the probability of detecting n photoelectrons obeys Mandel's equation (also known as the Poisson transform) to give the relation [6]:

$$p(N_{tot}) = \int_e^{-1} I_{tot}^N / N_{tot}! p(I) dI \tag{8}$$

For constant laser illumination, $p(I)$ degenerates into a delta function, leaving the familiar Poisson distribution for photoelectric counts. In GOPEX there are fluctuations in laser intensity from frame to frame[5] as well as from the atmosphere. Hence, the random nature of the photoelectron counts must include this second random factor. For any $p(I)$, intensity moments are related to those of photoelectron counts by the identities

$$< I > = < N_{tot} > \tag{9}$$

$$< I^2 > = < N_{tot}(N_{tot} - 1) > \tag{10}$$

$$\sigma_I^2 \ = < I^2 > - < I >^2 = \ \sigma^2{}_{N_{tot}} - < N_{tot} > \tag{11}$$

[5] G. Okamoto, "GOPEX Monitor Data Analysis," JPL Interoffice Memorandum 331.6-93-032 (internal document), Jet Propulsion Laboratory, Pasadena, California, February 3, 1993.

The corresponding lognormal variance based on the photoelectron counts is determined by the equations

$$\sigma_N{}^2 = \ln(1 + \sigma_I^2 / < I >^2) \tag{12}$$

with the lognormal mean following Eq. (16).

The most general probability distribution for the intensity fluctuation is the exponential distribution, and it represents the limiting distribution of modulation from the combination of all sources. Kiasaleh and Yan also recommend using this distribution in the presence of strong turbulence. In this limit, the photoelectrons follow the Bose–Einstein distribution whose mean and variance are

$$< N_{tot} > = \mu \tag{13}$$

$$\sigma^2_{N_{tot}} = \mu^2 + \mu \tag{14}$$

Using Eq. (12), the lognormal variance, σ_I^2 is always ln(2) and holds for all values of atmospheric turbulence.

There are further multiplicative factors, such as random atmospheric transmission, and other system parameters (see [3, Section II]) which could further broaden the distribution of photoelectric counts. An analysis by Saleh [7] produces an approximate solution for the detected light intensity after the signal has passsed through a channel with lognormally distributed disturbance characteristics. Its evaluation is beyond the scope of the analysis in this article, however, the exponential approximation should be adequate by assuming constant systematic conditions.

V. GOPEX Results and Discussion

Table 2 provides a summary of site operational conditions and data-derived results at TMF for GOPEX. The former includes the laser repetition rate, its beam divergence, range to Galileo, atmospheric seeing, and the gain state of the SSI. The latter includes the number of pulses detected (including pulses of zero intensity), $< N_{tot} >$, and the lognormal parameters, σ_I and m_n (using both theories). There appears to be good agreement between the data and the strong turbulence theory on day 1. This histogram of data pulses is plotted in Fig. 4. The error bars on the histogram heights show a relative range of probability that one would expect if another GOPEX data set, taken under the same conditions, were to be obtained and similarly displayed. The ± 1 standard-deviation error bars on the histogram are relatively wide due to the limited number of pulses available. As shown in Fig. 4, there is also good agreement between the data and the weak turbulence theory on day 2, the only day its assumptions were applicable in GOPEX. The weak turbulence approximation curve is close to most of the observed frequencies of pulses passing through most of the error bars of its histogram. The other histograms for TMF, Figs. 5–8, show varying agreement. On days 3 and 8, there is good agreement between the computed strong theory lognormal parameters and the data histograms. On day 6, the theory shows a good quantitative fit, but the lognormal fit due to the data does not agree as well. On day 7, there appears to be a bimodal histogram, which would indicate changing conditions during the experiment. For day 8, both histograms show a lack of fit near the smallest data bin. As mentioned in Section III.B, small values and zero values of the laser pulses were difficult to estimate, which probably downwardly biased this particular bin and artificially inflated the percentages of pulses in the other bins.

Table 3 similarly provides a summary of data and results for SOR. Note that the SOR seeing measurements are all in the strong turbulence regime and, consequently, weak theory estimates for the lognormal standard deviation and mean do not apply. The results are displayed in Figs. 9–12. One reason for the large differences between the data and the calculated lognormal moments differences is the lack of data. The best agreement between data and calculation was on day 4, and its histogram is shown below in Fig. 12. Again, there is an underestimation of the first histogram bin.

VI. Summary

Laser pulse data from the GOPEX demonstration have been analyzed for pulse strength and pulse distribution. Procedures were developed in both the weak turbulence regime and in the strong turbulence regime to fit the observed histogram of received pulses to a lognormal distribution. Both procedures were shown to quantitatively fit the data for a subset of data. Systematic differences between the data and lognormal fits obtained using atmospheric structure constant values computed from observatory seeing conditions and SSI camera conditions were attributed to the difficulty in determining small values and zero values of laser pulse energy measured by the SSI camera. Also, the use of nominal values of some attributes (like seeing, for example) as input parameters to the theoretical models may not have been representative of actual conditions. Pulse strengths could be measured with greater confidence if the relative location of pulses were

better known. The timing mismatch between the scan platform movement and the onset of laser pulse transmission deprived the analysis team of important information needed to determine the presence or absence of each pulse. Experimental sensitivity could also be improved through simple SSI camera calibrations. GOPEX was prevented from using such calibrations due to the lack of current data. At MIPL, extensive on-line software exists which uses the GALSOS program to perform this task once the calibration files are updated. The quality of the pulse intensity measurements could be improved, and possibly a greater number of data points could be obtained with the existing GOPEX image data set.

Acknowledgments

The authors are greatly indebted to the Multimission Image Processing Laboratory facilities and staff in general. In particular, the authors thank Lisa Wainio for providing staff for MIPL programming support and for providing the simulated images, and to Danika Jensen for her support during GOPEX operations and for providing all the images used in the analysis. The authors also acknowledge discussions with Keith Wilson, Jim Lesh, and Jim Anderson on data analysis, and the support of Gregory Wanish for his help with critical parts of the MATLAB programming.

References

[1] K. E. Wilson and J. R. Lesh, "An Overview of the Galileo Optical Experiment (GOPEX)," *The Telecommunications and Data Acquisition Progress Report 42-114, vol. April–June 1993*, Jet Propulsion Laboratory, Pasadena, California, pp. 192–204, August 15, 1993.

[2] MATLAB, Natick, Massachusetts: MathWorks, Inc., 1992.

[3] K. Kiasaleh and T.-Y. Yan, "A Statistical Model for Evaluating GOPEX Uplink Performance," *The Telecommunications and Data Acquisition Progress Report 42-111, vol. July–September 1992*, Jet Propulsion Laboratory, Pasadena, California, pp. 325–332, November 15, 1992.

[4] V. I. Tatarski, *Wave Propagation in a Turbulent Medium*, New York: McGraw Hill, 1961.

[5] J. W. Goodman, *Statistical Optics*, Chapter 8, New York: John Wiley and Sons, 1985.

[6] J. W. Goodman, *Statistical Optics*, Chapter 9, Sections 9.1 and 9.2, New York: John Wiley and Sons, 1985.

[7] B. E. A. Saleh, *Photoelectron Statistics*, Section 5.2, p. 242, New York: Springer-Verlag, 1978.

Table 1. Data reduction for GOPEX data frame 8 on day 2.

Results for file = Day 2/sec 0165359600.1

Transmitter location = SOR

Pulse number	Peak position		Centroid position		Distance	Background signal	Corrected dn in 25 pixels	Comments
	Row	Col.	Row	Col.	Pixel	dn per pixel		
1	557	325	556.91	325.01	0.0	23.9	352.0	—
2	614	325	613.96	325.01	57.1	22.9	168.5	—
3	671	325	670.99	324.97	57.0	21.7	247.5	—
4	729	326	727.76	325.78	56.8	75.8	409.0	—
5	785	325	785.45	324.98	57.7	34.8	100.0	—

Transmitter location = TMF

Pulse number	Peak position		Centroid position		Distance	Background signal	Corrected dn in 25 pixels	Comments
	Row	Col.	Row	Col.	Pixel	dn per pixel		
1	510	377	510.66	377.00	0.0	64.2	21.0	—
2	547	377	548.07	377.06	37.4	59.1	196.5	—
2[a]	—	—	—	—	—	21.2	44.0	Replace above
3	585	377	585.02	376.99	36.9	20.1	28.0	—
4	623	377	622.99	376.97	38.0	19.7	45.5	—
5	660	377	660.02	376.98	37.0	19.1	21.5	—
5.1[b]	698	377	—	—	38	18.2	28.0	On 2×3 between RS[c] errors
5.2[b]	736	377	—	—	38	17.0	16.0	On 2×3 between RS errors
6	774	377	772.54	376.99	112.5	60.9	36.0	Signal okay

[a] Replace background signal and corrected signal in 2.

[b] Pulse found by manual inspection.

[c] RS = Reed Solomon.

Table 2. GOPEX data results summary at TMF on days data were received.

Parameter	Day 1	Day 2	Day 3	Day 4	Day 6	Day 7	Day 8
Site and spacecraft conditions							
Repetition rate, pulses/sec	15	15	30	—	30	30	30
Beam divergence, μrad	110	110	110	—	60	60	60
Average range, $\times 10^6$ km	0.7	1.45	2.21	—	4.48	5.25	6.01
Average zenith angle, deg	50	51	53	—	55	56	56
Seeing due to turbulence, μrad	20	7.5	20	—	40	20	30
SSI camera gain state, electrons/dn	391	391	156	—	156	156	156
Data products							
Data frames received	60	40	20	—	12	10	8
Number of frames with pulse detections	10	16	5	—	3	6	6
Total received pulses	33	59	41	—	24	60	51
Expected photoelectrons/pulse, μ	67,116	14,860	7267	—	4352	3295	2629
Lognormal mean, m_l (data)	10.86	9.27	8.45	—	7.70	8.36	7.41
Lognormal mean, m_l (strong theory)	10.83	—	8.50	—	8.03	7.75	7.36
Lognormal mean, m_l (weak theory)	—	9.40	—	—	—	—	—
Lognormal standard deviation, σ_N (data)	0.7263	0.5356	0.940	—	1.047	0.8060	0.8619
Lognormal standard deviation, σ_N (strong theory)	0.8326	—	0.8326	—	0.8326	0.8326	0.8326
Lognormal standard deviation, σ_N (weak theory)	—	0.6300	—	—	—	—	—

Table 3. GOPEX data results summary at SOR on days data were received.

Parameter	Day 1	Day 2	Day 3	Day 4	Day 6	Day 7	Day 8
Site and spacecraft conditions							
Repetition rate, pulses/sec	10	10	10	10	—	—	—
Beam divergence, μrad	80	80	80	10	—	—	—
Average range, $\times 10^6$ km	0.7	1.45	2.21	4.48	—	—	—
Average zenith angle, deg	50	51	53	54	—	—	—
Seeing due to turbulence, μrad	No data	13.5	13.5	17.0	—	—	—
SSI camera gain state, electrons/dn	391	391	156	156	—	—	—
Data products							
Data frames received	60	40	20	10	—	—	—
Total received pulses	16	43	12	8	—	—	—
Expected photoelectrons/pulse, μ	74,818	17,178	7233	3447	—	—	—
Lognormal mean, m_n (data)	10.49	10.64	8.70	8.07	—	—	—
Lognormal mean, m_n (strong theory)	10.88	9.41	9.23	7.80	—	—	—
Lognormal mean, m_n (weak theory)	—	9.40	—	—	—	—	—
Lognormal standard deviation, σ_N (data)	1.0153	0.7360	0.9613	0.8505	—	—	—
Lognormal standard deviation, σ_N (strong theory)	0.8326	0.8326	0.8326	0.8326	—	—	—
Lognormal standard deviation, σ_N (weak theory)	—	—	—	—	—	—	—

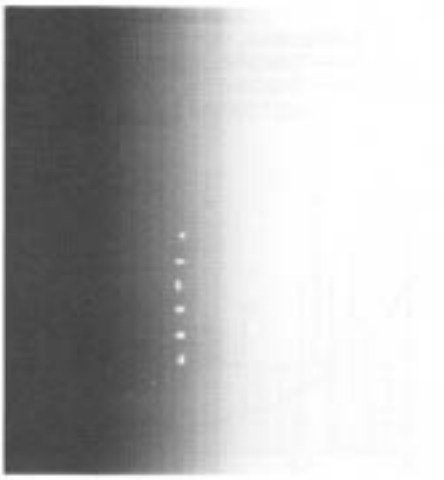

Fig. 1. A portion of a simulated image for day 1 of GOPEX.

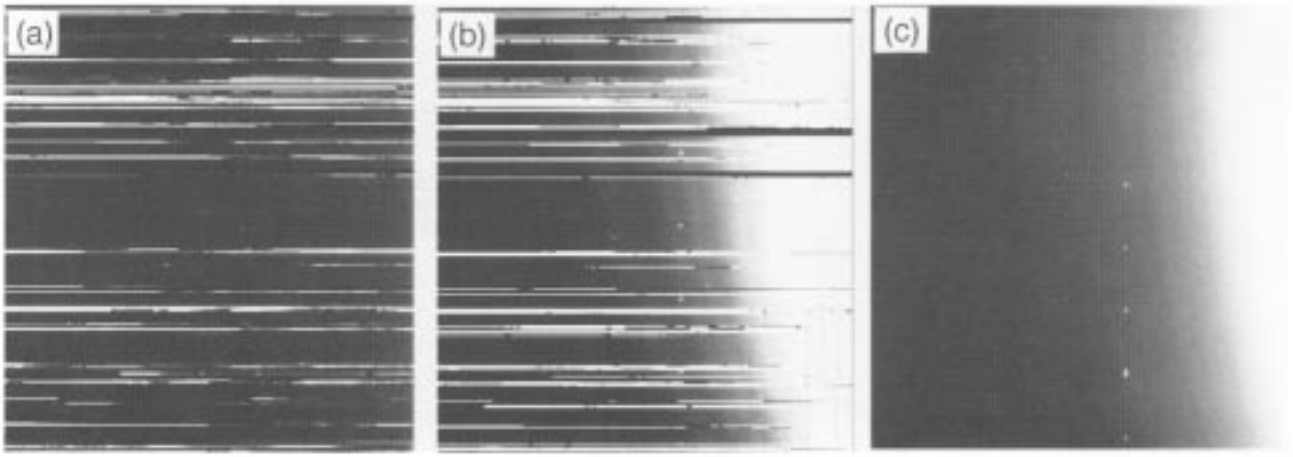

Fig. 2. Raw and processed GOPEX images for day 2, frame 8: (a) raw 8-bit image; (b) contrast stretched image; and (c) MIPL-processed image.

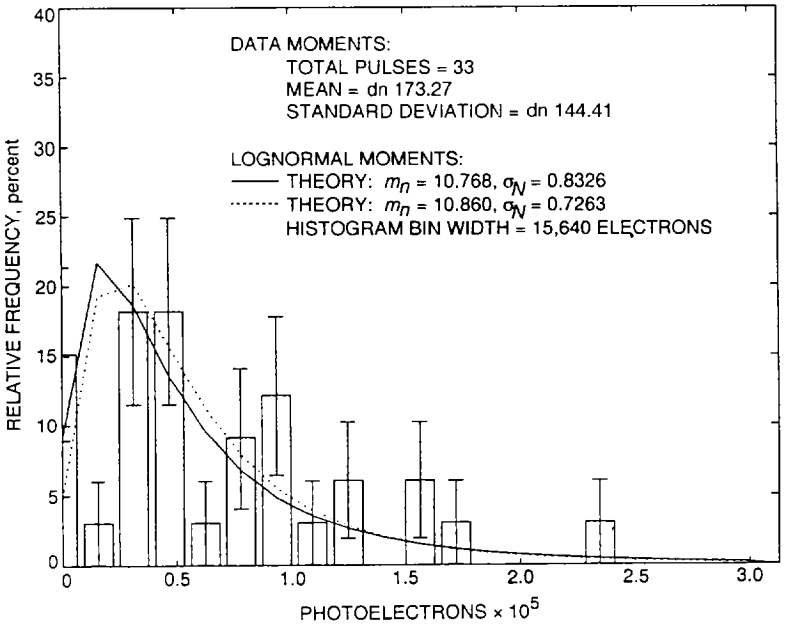

Fig. 3. Histograms for TMF on day 1 of GOPEX. Using the lognormal model, strong turbulence theory parameters agree well with the data parameters.

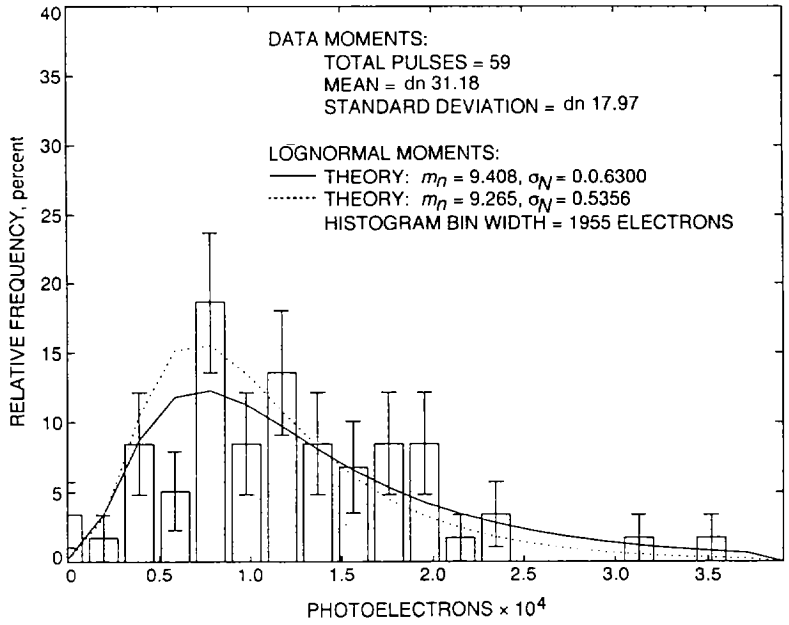

Fig. 4. Comparison of weak turbulence theory for day 2 of GOPEX, at TMF; histogram fit using weak turbulence theory. The error bars represent ±1 standard deviation.

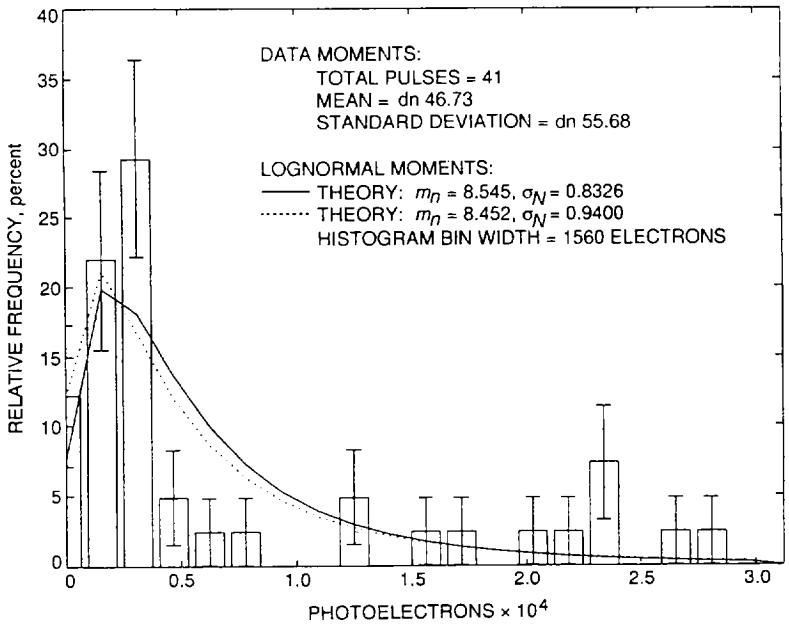

Fig. 5. Histograms for TMF on day 3 of GOPEX.

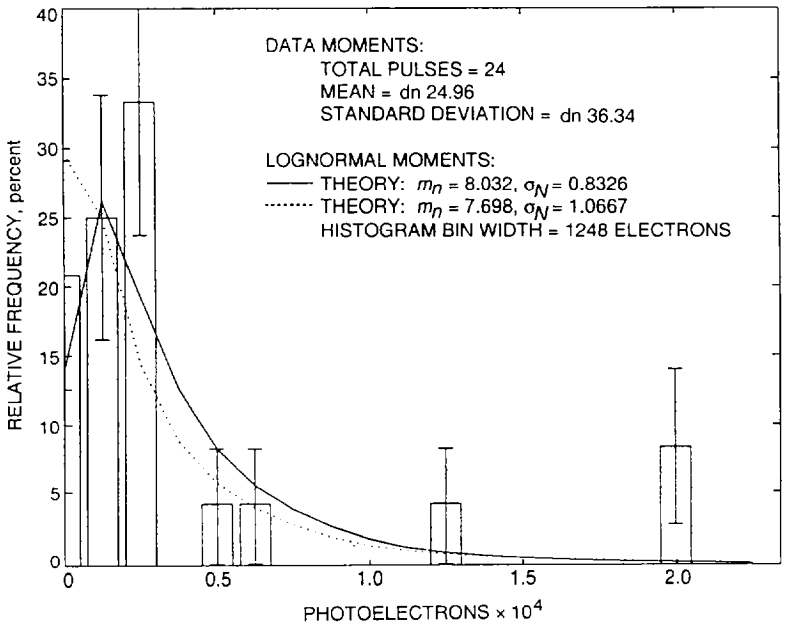

Fig. 6. Histograms for TMF on day 6 of GOPEX.

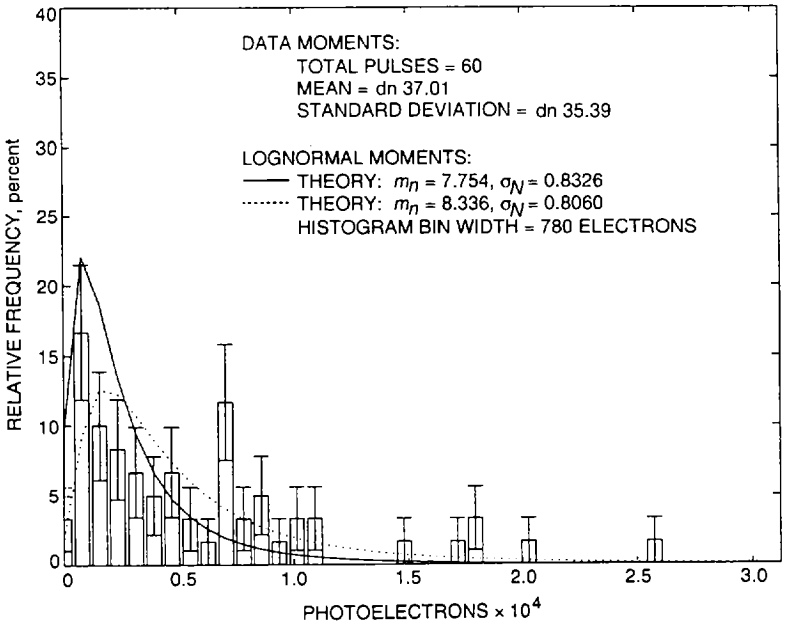

Fig. 7. Histograms for TMF on day 7 of GOPEX.

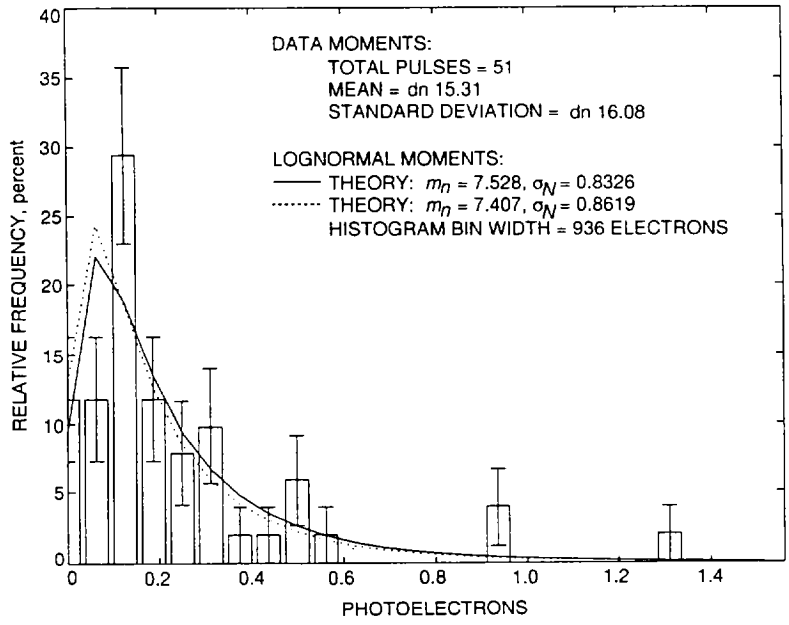

Fig. 8. Histograms for TMF on day 8 of GOPEX. There is good agreement between the data and the lognormal distribution using strong turbulence theory parameters.

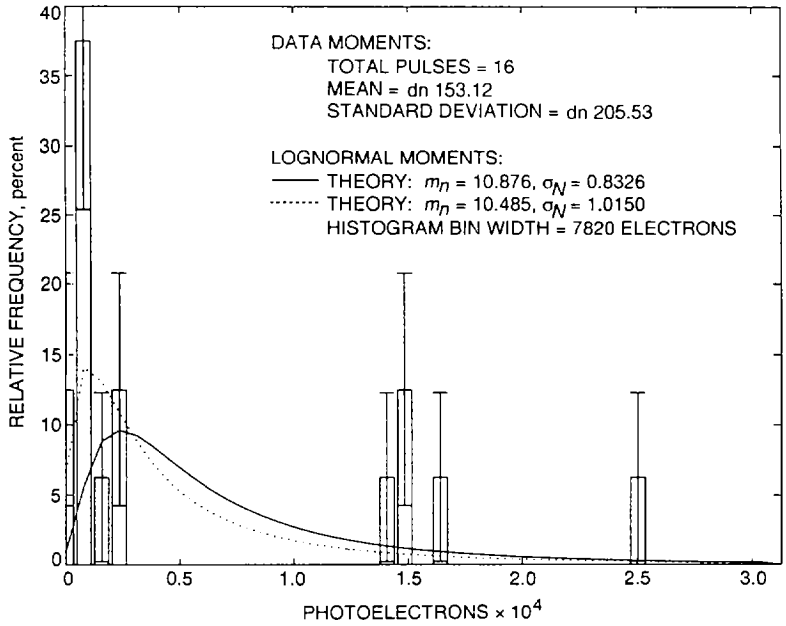

Fig. 9. Histograms for SOR on day 1 of GOPEX.

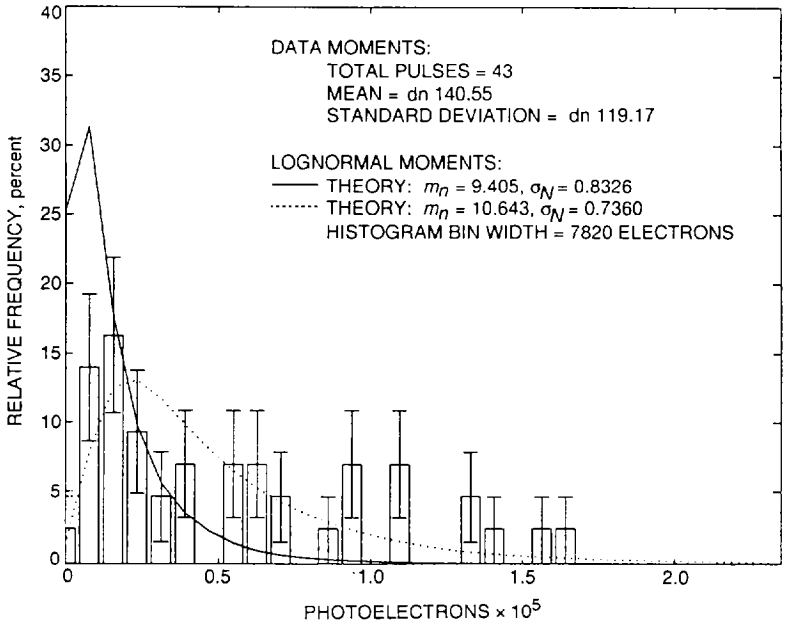

Fig. 10. Histograms for SOR on day 2 of GOPEX.

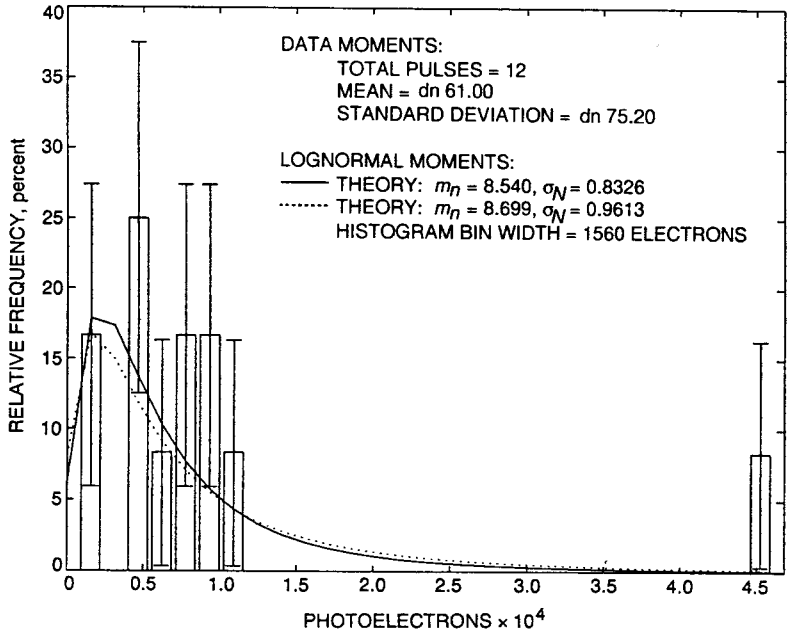

Fig. 11. Histograms for SOR on day 3 of GOPEX.

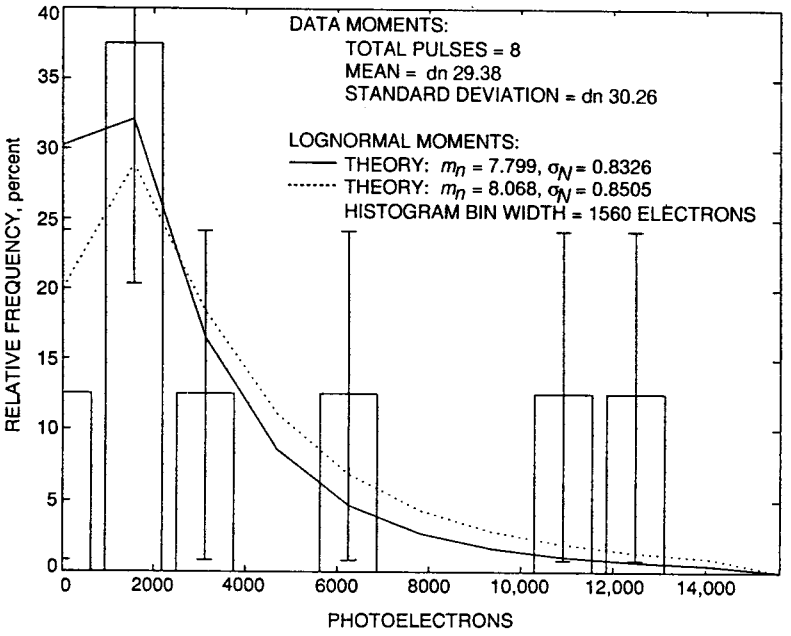

Fig. 12. Histograms for SOR on day 4 of GOPEX.

Appendix

Figures A-1 and A-2 are MATLAB m-files written to plot the observed frequency histogram with its error bars and to compare the data to the lognormal distribution with parameters given by either the weak or strong turbulence theories. The first m-file evaluates the lognormal probability density function, and the second m-file compiles the histogram, error bars, and directs the plotting.

The MATLAB m-file for computing the lognormal probability density function for a vector of photoelectric counts given by x is presented in Fig. A-1.

The MATLAB m-file for plotting the histogram and its related error bars with the lognormal probability density function using parameters derived from either the data or theory is presented in Fig. A-2.

```
function fx=log_norm(mu,sigma,x)
%bml 21 dec 92
%evaluates the lognormal distribution function over the vector x (xmin>0)
%parameters of the log normal are mu and sigma
%
fx=[];
n=size(x,2);
fact=sqrt(2.*pi).*sigma;
fact2=2*sigma*sigma;
mean=mu.*ones(1,n);
arg=fact.*x;
arg2=(log(x)-mean).*(log(x)-mean)./fact2;
fx=exp(-arg2)./arg;
```

Fig. A-1. The MATLAB m-file for computing the lognormal probability density function for a vector of photoelectric counts given by *x*.

```
function des_stat=histo_theory2(freq,xmitr,day,deltab,bmax,gain,mu,sigma)
% output file names fileroot=[day, '.',xmitr,'.'];
% descriptive statistics small=min(freq);
large=max(freq);
avg=mean(freq);
med=median(freq);
stdev=std(freq);
%
%histogram plot
%assumes a vector of intensities
bins=0:deltab:bmax;
[count location]=hist(freq,bins);
%normalize counts total=sum(count);
ndata=total;
count=100.*count./total;
%plot results bar(location,count);
axis([0 bmax 0 60]);
xlabel('DN');
ylabel('relative frequency (%)');
title_string=sprintf('GOPEX encircled energy at %s; %s--bins=%2i DN, Total=%3i
pulses',xmitr,day,deltab,ndata); title(title_string);
%keyboard
print_command =['print ',fileroot,'DN.ps'];


draft filed as: /var8/gopex/memos/tda-image.report
last revision: February 24, 1993 1:55 pm
eval(print_command)
%
%theory lognormal pdf
delta=deltab*gain;
cmax=gain*bmax;
counts=gain.*freq;
bins=0:delta:cmax;
[count location]=hist(counts,bins);
%normalize counts total=sum(count);
count=100.*count./total;
%plot results
x=1:cmax;
pdf1=log_norm(mu,sigma,x);
%integrate over bin width
nbins=floor(cmax/delta);
for i=1:nbins
  pdf(i)=100*sum(pdf1((i-1)*delta+1:i*delta));
end
```

Fig. A-2. The MATLAB m-file for plotting the histogram and its related error bars with the lognormal probability density function using parameters derived from either the data or theory.

```
pdf=[pdf'; 100*sum(pdf1(nbins*delta+1:cmax))]';
%sample lognormal pdf
sigma2=sqrt(log(stdev*stdev/avg/avg+1));
mean2=log(avg*gain)-sigma2*sigma2/2;
pdf1=log_norm(mean2,sigma2,x);
%integrate over bin width
nbins=floor(cmax/delta);
for i=1:nbins
  sample_pdf(i)=100*sum(pdf1((i-1)*delta+1:i*delta));
end
sample_pdf=[sample_pdf'; 100*sum(pdf1(nbins*delta+1:cmax))]';
%plot results
ebar=100.*sqrt(count.*(100.-count)./10000./total);
errorbar(location,count,ebar);
hold on;
plot(location,count,'k');
bar(location,count);
axis([0 cmax 0 40]);
xlabel('photoelectrons');
ylabel('relative frequency (%)');
%keyboard
title_string=sprintf('GOPEX encircled energy for %s on %s',xmitr,day); title(title_string);
plot(bins,pdf);
plot(bins,sample_pdf,':');
string1=sprintf('data moments:  total pulses = %3i', ndata);
string2=sprintf('mean     = %5.2f DN  std dev  =%5.2f DN',avg,stdev);
string3=sprintf('log normal moments');
string4=sprintf('theory:  mN  = %6.3f  sigmaN = %7.4f',mu,sigma);
string5=sprintf('data   :  mN  = %6.3f  sigmaN = %7.4f',mean2,sigma2);
string6=sprintf('histogram bin width = %g electrons',delta); x=.4*cmax;
text(x,39,string1);
text(x,37,string2);


draft filed as: /var8/gopex/memos/tda-image.report
last revision: February 24, 1993 1:55 pm
text(x,34,string3);
plot ([x-.05*cmax; x-.005*cmax],[32; 32]);
text(x,32,string4);
plot ([x-.05*cmax; x-.005*cmax],[30; 30],':');
text(x,30,string5);
text(x,28,string6);
% output histogram
print_command =['print ',fileroot,'counts.ps'];
eval(print_command)
%print counts.ps
hold off;
%save day2.histogram.mat bins freq
des_stat=[small; large; med; avg; stdev];
```

Fig. A-2. (Cont'd)